BIOCHEMISTRY

 Volume 47, Number 40 October 07, 2008

Articles

Helix−Helix Interactions in Membrane Proteins: Coarse-Grained Simulations of Glycophorin A Helix Dimerization[†]

Emi Psachoulia, Philip W. Fowler, Peter J. Bond,[‡] and Mark S. P. Sansom*

Department of Biochemistry, University of Oxford, South Parks Road, Oxford OX1 3QU, U.K.

Received April 17, 2008; Revised Manuscript Received July 3, 2008

ABSTRACT: Oligomerization of transmembrane (TM) helices is a key stage in the folding of membrane proteins. Glycophorin A (GpA) is a well-documented test system for this process. Coarse-grained molecular dynamics (CG-MD) allows us to simulate the self-assembly of TM helices into dimers, for both wild-type (WT) and mutant GpA sequences. For the WT sequences, dimers formed rapidly and remained stable in all simulations. The resultant dimers exhibited right-handed crossing and the same interhelix contacts as in NMR structures. Simulations of disruptive mutants revealed the dimers were less stable, with values of $\Delta\Delta G_{\mathrm{dimerization}}$ consistent with experimental data. The dimers of disruptive mutants were distorted relative to the WT and showed left-handed crossing of their helices. CG-MD can therefore be used to explore the interactions of TM helices, an important stage in the folding of membrane proteins. In particular, CG-MD has been shown to be sensitive enough to detect disruptions introduced by mutation. Future refinement of such models via atomistic simulations will enable a multiscale approach to predict the folding of membrane proteins.

Membrane proteins play a key role in most cellular processes such as trafficking, signaling, and transport. While they account for ∼25% of open reading frames in most genomes (*1*), only ∼100 high-resolution structures of membrane proteins are known (see http://blanco.biomol.uci.edu/Membrane_Proteins_xtal.html for a summary). From the structures that have been determined, it is evident that there are two basic folds for the transmembrane (TM)[1] domain of a membrane protein: these are a bundle of α-helices or an antiparallel β-barrel. The α-helical bundles are the major class, and they are thought to assemble according to the two-stage folding model (*2*), in which the α-helices insert independently into the membrane, before self-assembling into a functional helix bundle. Understanding the second stage may enable the prediction of membrane protein structures to be improved (*3*), as well as advancing our knowledge of their folding and assembly (*4*). It is of particular interest to establish the specific interactions between α-helices that are necessary for maintaining the final tertiary structures of helical bundle membrane proteins and also to understand how disrupting these interactions by mutation leads to misfolding (*5*). Recent studies of the structure of the translocon (*6*) and of the mechanism of translocon-mediated insertion of membrane proteins (*7*) also stress the role of TM helices and their dimerization.

[†] This work was supported by grants from the BBSRC and the Wellcome Trust.

* To whom correspondence should be addressed. E-mail: mark.sansom@bioch.ox.ac.uk. Tel: +44-1865-275371. Fax: +44-1865-275273.

[‡] Current address: Max Planck Institute of Biophysics, Max-von-Laue-Str. 3, 60438 Frankfurt/Main, Germany.

[1] Abbreviations: RMSD, root mean square deviation; GpA, glycophorin A; TM, transmembrane; WT, wild type; CG-MD, coarse-grained molecular dynamics; AT, atomistic.

10.1021/bi800678t CCC: $40.75
Published on Web 09/11/2008

Glycophorin A (GpA) has served as a model for studying TM membrane protein structure and stability, from both an experimental (*8*−*15*) and a computational (*16*−*25*) perspective. GpA is homodimeric; each chain consists of 131 amino acids and spans the membrane once such that its amino terminus is at the extracellular surface of the human red blood cell. Its single TM domain consists of ~25 residues that adopt an α-helical conformation and are sufficient for dimerization (*13*). Structures of this homodimeric TM domain have been determined in detergent micelles (*10*) and lipid bilayers (*14, 26*). The TM region contains a seven-residue motif, LIxxGVxx-GVxxT (residues 75−87), which plays a key role in homodimerization (*27*). In particular, it stabilizes the packing of the helices in a right-handed fashion, with a negative crossing angle (*13*).

Mutational screens have been used to probe the interface of the GpA dimer (*28*). In general, it has been found that replacement of the small or polar residues G79, G83, or T87 in the key dimerization motif with larger nonpolar residues disrupts dimerization. The G79L, G83L, and T87F mutations are three mutations that significantly disrupt dimerization (*8, 13, 28, 29*). The NMR structures in both solution (*10*) and lipid bilayers (*14*) reveal that G79 and G83 are involved in maintaining the proximity of the helices and enabling intimate contacts between other interhelical side chains to be formed (*27*), leading to a right-handed crossing angle for the dimer (*13, 27*). The G79L and G83L mutations presumably prevent dimerization by introducing bulkier side chains at positions 79 and 83, thus abolishing the flat interaction surface necessary for the packing of other nearby side chains in the helix−helix interface (*27*). Additionally, one of ensembles of NMR structures (*14, 26*) suggests that the side chain hydroxyl group of T87 in the key dimerization motif is involved in an interhelical hydrogen bond across the dimer interface. This bond has been shown experimentally to be important for the stability of the dimer (*30*), thus explaining the effect of the T87F mutation. Finally, mutations such as A82W and I85F have no effect upon dimerization, presumably because their side chains are located distal to the helix−helix interface (*30*).

Molecular dynamics (MD) simulations provide a computational tool for probing the structure and dynamics of membrane proteins in detergent micelles (*31*) and lipid bilayers (*32*). Several simulations of GpA have been performed in both detergent micelles (*19, 33*) and lipid bilayers (*16, 22*). Moreover, atomistic MD simulations (*21*) and docking-based methods (*34*) have been used to estimate the energetics of helix dimerization. The spontaneous self-assembly of GpA/detergent systems has been studied using extended atomistic MD simulations (*19, 33*). Atomistic simulations have also been used to investigate the self-assembly of helix bundles and the roles of interhelical H-bonds in the stabilization of TM helix oligomers (*35*). In general, however, longer time scales than those accessible by atomistic simulation are necessary to fully characterize complex processes such as helix−helix dimerization. This is possible with a coarse-grained (CG) approach (*36*−*42*), in which small groups of atoms are treated as single particles, allowing longer time scales and larger systems to be simulated. A recent CG model has been used to model the spontaneous self-assembly of GpA monomers into dimers within detergent micelles and lipid bilayers (*25*).

The aim of this paper is to determine the extent to which CG-MD simulations may be used to explore and predict the effects of mutations on the stability of TM helix interactions. We shall present and compare the results of simulations using CG-MD of the dimerization of TM helices of wild-type (WT) and mutant GpA within lipid bilayers. By running multiple extended simulations, we find that it is possible both to predict in a semiquantitative manner and to characterize the effects of each mutation on the stability of the dimers. The resultant correlation with experimental data is encouraging and permits a structural rationalization of the effects of mutations in the GxxxG helix dimerization motif. This approach is also a direct and novel method for estimating in a semiquantitative manner the $\Delta\Delta G$ of association of TM helices in lipid bilayers using CG-MD simulations.

MATERIALS AND METHODS

Initial Helix Structures. The structure of GpA from a solution/micelle NMR study (PDB 1AFO) (*10*) provided the initial structure of a GpA TM helix *monomer*; this was used as the starting point for all simulations. Models of the mutant TM helices were derived from this structure using MODELLER 7v7 (*43*). These atomistic structures were converted to corresponding CG models as described previously (*25, 40*) using a modified version of the Marrink CG force field (*37*). The coarse graining of amino acids was based on the methods developed for lipids by Marrink et al. (*37*). In this CG force field an approximate 4:1 mapping of heavy (i.e., not H) atoms to CG particles is used. Four major CG particle types are distinguished: polar (P), mixed polar/apolar (N), hydrophobic apolar (C), and charged (Q). There are further subtypes for the N and Q particles which allow fine-tuning of the Lennard-Jones interactions to reflect hydrogen-bonding capabilities. Initial simulations showed that the existing CG force field did not reproduce well the right-handed orientation of wild-type GpA dimers. The CG force field was therefore refined compared to the version used previously (*25, 40*) to correct this defect. Specifically, the particle type of the backbone particle of glycine was changed from N0 to Nm. This makes it more likely that neighboring glycines will interact since while N0−N0 pairwise interactions are "intermediate" in nature, Nm−Nm pairwise interactions are "semiattractive". This change is intuitive since the backbone of glycine is more exposed and therefore can more readily interact with other residues.

Simulation Methods. CG simulations were performed using GROMACS (www.gromacs.org) (*44*) as described in refs *25* and *40* with CG parameters for lipid molecules (dipalmitoylphosphatidylcholine, DPPC) and water molecules as in ref *37* and for amino acids as in refs *25* and *45* modified as described above. A CG peptide or protein model was generated from the corresponding atomistic structure and was composed of a chain of backbone particles with attached side chain particles. Protein bond and angle potentials are described in the Supporting Information of ref *46*. Lennard-Jones interactions were shifted to zero between 9 and 12 Å, and electrostatics were shifted to zero between 0 and 12 Å, with a relative dielectric constant of 20. The nonbonded neighbor list was updated every 10 steps. All simulations were performed at constant temperature, pressure, and number of particles. The temperatures of the protein, lipid,

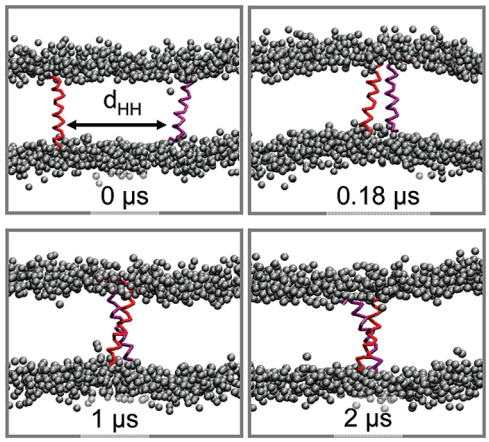

FIGURE 1: Progress of a WT GpA TM helix dimer simulation. Run 1 of the ensemble of seven WT simulations is illustrated. The initial system configuration (0 μs) consists of two helices (red and purple) preinserted in a DPPC bilayer in a parallel orientation with an interhelix separation of $d_{HH} \sim 55$ Å. The choline, phosphate, and glycerol backbone particles of the DPPC molecules are shown in silver. Subsequent snapshots illustrate the simulation at 0.18, 1, and 2 μs.

and solvent were each coupled separately using the Berendsen algorithm (*47*) at 323 K, with a coupling constant $\tau_T = 1$ ps. The system pressure was semiisotropically coupled in the *x*, *y*, and *z* directions using the Berendsen algorithm at 1 bar with a coupling constant $\tau_P = 1$ ps and a compressibility of 5×10^{-6} bar^{-1}. The time step for integration was 20 fs. Coordinates were saved for subsequent analysis every 200 ps. Note that the coarse-grained time scale was calibrated by, for example, measuring the diffusion constant of water (*45*), and therefore other time scales, for example, diffusion in lipids, may be under- or overestimated. This is irrelevant here as our analyses and conclusions are independent of time. Analysis of all simulations was performed using the GROMACS suite of programs. VMD (*48*) and xfarbe were used for visualization and graphics.

Simulation Systems. Seven simulations of the GpA-WT helices and of each mutant were performed. The mutants were specifically chosen to satisfy two criteria: (i) a disruptive effect of the mutation on dimerization has been observed experimentally, and (ii) there is a significant difference between the CG parameters of the wild type and the mutated residues in terms of both number and type of particles. A further two mutants were chosen which do *not* disrupt the formation of dimers and were consequently used as controls. For all simulations, two helices were inserted in a preformed DPPC bilayer containing 245 lipids such that they were separated by ~55 Å (Figure 1). Following energy minimization using up to 100 steps of the steepest descent method, each system was solvated with 2241 CG water particles. The energy of each system was again minimized, and seven 3 μs simulations were run for the GpA-WT and mutant sequences; each set of simulations was started from the same configuration but with different random seeds.

Analysis of Dimer Stability. The stabilities of the mutant helix dimers relative to the WT were expressed as $\Delta\Delta G$ values calculated as follows: (1) The initial helix association period was discarded for each trajectory. (2) The seven resultant trajectories were merged. (3) The total number of dimeric (n_{dimer}) and monomeric ($n_{monomer}$) conformations were counted. Two helices are defined to be a dimer when the closest contact distance, d_{HH}, is less than 6 Å. Altering this arbitrary cutoff does not materially affect the results (data not shown). (4) The association equilibrium constant, assuming that the probability of a state is given by the number of molecules in that state relative to the total number of molecules, is given by $K = (n_{dimer})/(n_{monomer})^2(1/n_{tot})$. (A more complete description of the derivation of this can be found in the Supporting Information.) In the above equation $(1/n_{tot})$ defines the standard state which cancels out in the equation for $\Delta\Delta G$. (5) Thus, for each mutant, $\Delta\Delta G = RT \ln(K_{WT}/K_{mutant})$ where T is the temperature (323 K) and R is the universal gas constant.

Table 1: Sequences of the GpA TM Helix and Its Mutants

GpA helix	TM sequence	dimerization[a]
WT	ITLIIFGVMAGVIGTILLISYGI	dimer
G83L	ITLIIFGVMALVIGTILLISYGI	no dimer
T87F	ITLIIFGVMAGVIGFILLISYGI	no dimer
G79LG83L	ITLIIFLVMALVIGTILLISYGI	no dimer
A82W	ITLIIFGVMWGVIGTILLISYGI	dimer
I85F	ITLIIFGVMAGVFGTILLISYGI	dimer

[a] Derived from data in refs *8* and *28*. Residues suggested to play a key role in the dimerization of the GpA TM helix are in bold; the mutated residues are underlined.

The trajectories of the seven simulations were merged because the individual trajectories had not fully converged and therefore could not be used to estimate thermodynamic parameters. We are therefore assuming that the merging process improves convergence and allows us to estimate thermodynamic parameters. This procedure also assumes that we can construct a statistical mechanical ensemble of monomer and dimer conformations from our simulations. We are implicitly assuming that the ergodic hypothesis holds and that the time average is the same as the ensemble average.

RESULTS

Simulations Performed. Snapshots from an example CG simulation are given in Figure 1. The two GpA α-helices were inserted in a parallel orientation into a preformed dipalmitoylphosphatidylcholine (DPPC) bilayer with the helices separated by a distance, d_{HH}, of ~55 Å. Each simulation was then run for 3 μs, during which time the TM helices diffused randomly in the bilayer, encountered one another, and interacted. Simulations have been performed for the WT 23-mer TM helix of GpA and for five mutant TM sequences (Table 1). For each of these different sequences seven simulations were run. Three of the mutants (G83L, T87F, G79LG83L) have been shown by experiment to destabilize the GpA TM helix dimer. The other two mutants (A82W and I85F) still formed dimers in experiments and so were used as positive controls.

Wild-Type GpA. As observed in earlier self-assembly simulations (*25*) the WT GpA TM helices spontaneously form a long-lasting helix dimer (Figure 1) within a few hundred nanoseconds. Examination of representative structures of the WT dimer (Figure 2A) reveals that the helices are packed in a right-handed fashion (i.e., have a negative value of the helix-crossing angle Ω) with the G79, G83, and T87 residues forming the helix−helix interface, as indicated by NMR structures (*10, 14, 26*) and by mutagenesis data (*8, 27*−*29*).

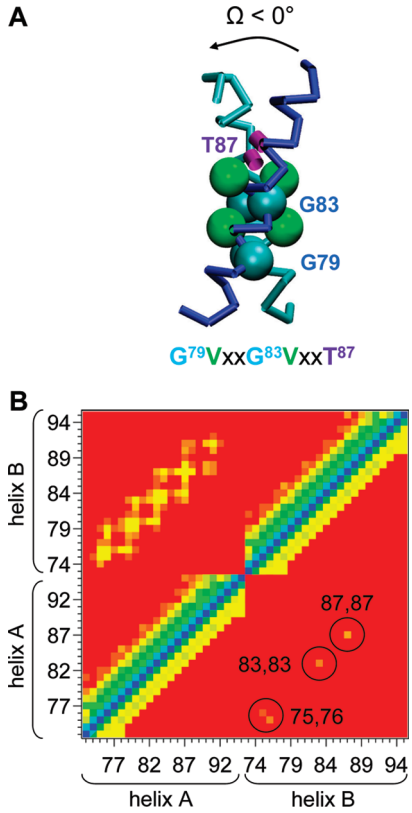

FIGURE 2: Helix−helix contacts in the WT GpA TM helix dimer. (A) Representative structure from the WT ensemble showing the negative (i.e., right-handed) helix crossing angle (Ω) and key interfacial residues. The backbone particles (cyan) are shown for G79 and G83. The side chain particles are shown for V80 and V84 (green spheres) and for T87 (purple rods). (B) Interhelix contact matrices for the WT simulation ensemble calculated using a 10 Å (upper half) and 8 Å (lower half) distance cutoff. The colors indicate the distances (all particles) of the contacts ranging from 0 Å (blue) to 10 or 8 Å (red). For the lower half of the matrix key interhelix contacts are circled.

Helix−helix contacts were examined in more depth by calculating the interhelix distance matrices averaged over all seven WT simulations (Figure 2B). From this it is evident that the interactions are dominated by the key residues of the $L^{75}IxxG^{79}VxxG^{83}VxxT^{87}$ motif (*8, 10, 28, 29*). Thus, the most prominent interactions are between residues 75 and 76, 79 and 80, 83 and 84, and 87 and 87.

The formation of a GpA dimer may be monitored by plotting d_{HH} as a function of time (Figure 3). In all of the seven WT simulations, the helices formed a dimer in the first 500 ns and remained a dimer for the majority of the remainder of each simulation. Indeed, in four of the simulations, the dimer did not dissociate at all during the simulation. In the other three WT simulations some transient dissociation of the helices was observed, but in all cases the dimer re-formed. The individual trajectories are not fully converged; as described in the Materials and Methods we therefore merged the trajectories and analyzed the resulting data. Once the helices have formed a dimer, the number of conformations spent in the dimeric state relative to the number of conformations spent in the monomeric state therefore provides a semiquantitative measure of the stability of the dimer. This will be explored further below by comparing the WT helix to the mutant helices.

While the aim of this paper is not to study the diffusion of GpA helices in a lipid bilayer in detail, we shall briefly

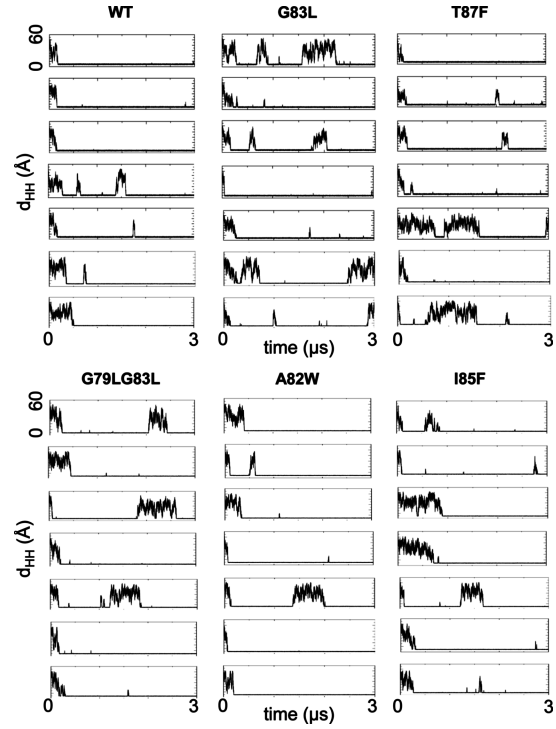

FIGURE 3: Interhelix separations of WT and mutant GpA simulations. The interhelix separation d_{HH} (defined as the closest approach distance of the two helices) is shown as a function of time for all of the simulations.

examine a WT and a mutant simulation to illustrate how the CG helices move in a lipid bilayer. The following analysis is in the frame of reference of the lipid bilayer where one of the helices is held at a fixed point. The position of the center of mass of each helix is plotted for the representative WT simulation in Figure 4A. The mobile helix appears to diffuse randomly until it binds to the fixed helix. Since this analysis is in the frame of reference of the bilayer, the fixed helix is free to rotate around the *z*-axis, and therefore we cannot draw any conclusions from this analysis about the precise spatial orientation of the two helices relative to one another. To investigate this, the dimer conformations from all of the simulations were combined, and the spatial distribution of the mobile helix was measured (Figure 5). The position of the mobile helix is anisotropically distributed and favors one side of the fixed helix.

It is interesting to compare the structures of the dimer from the WT simulations with a solution NMR structure in a detergent micelle (*10*) and a solid-state NMR-derived model in a lipid bilayer (*14*). We shall do this by evaluating the root mean square deviation (RMSD) for the backbone particles of the residues comprising the GpA dimerization motif (i.e., residues from L75 to T87 inclusively) between the simulations and the NMR structures (Table 2). The mean value of 3.6 Å for the comparison between structures drawn from the WT simulations and the solution/micelle NMR structure (*10*) might suggest that on average the structures generated by simulation do not closely resemble the experimental structure. This, however, hides a wide range variation in individual RMSD values; i.e., there are some structures from the simulations that are very similar to the experimental structure and are some that are different. This can be seen in the high value of the standard deviation (1.3 Å) and is also to be expected when we consider the relative spatial

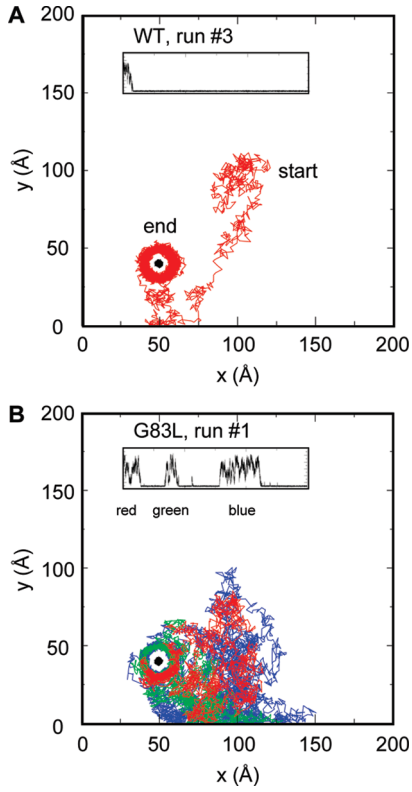

FIGURE 4: Example motions of one GpA helix relative to the other in the reference frame of the lipid bilayer. The positions of the centers of mass of a WT simulation (run 3) and a G83L simulation (run 1) are plotted in (A) and (B), respectively. The positions of the fixed helices are drawn in black. The coordinates (x, y) of the mobile helix are drawn in red for the wild type and in red, green, and blue for the G83L mutant to distinguish the unbinding events. Note that the fixed helix is free to rotate, and therefore its coordinates describe a ring.

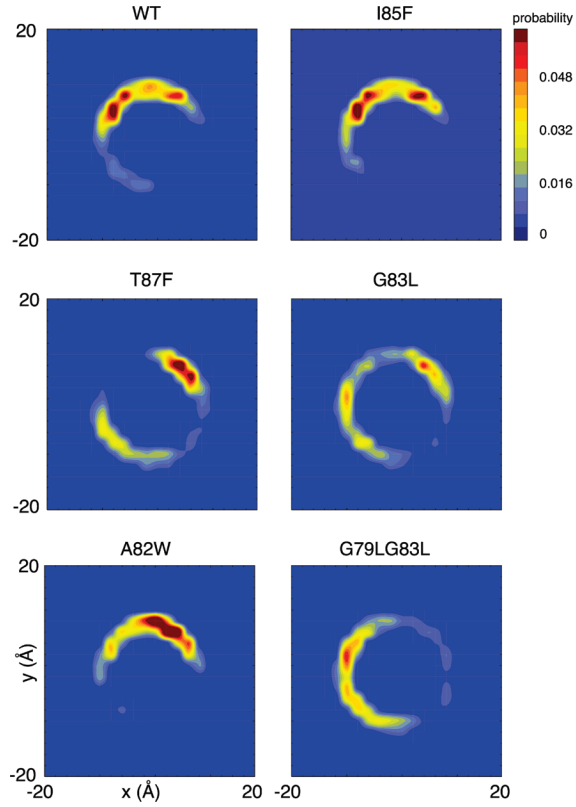

FIGURE 5: Spatial distributions of one GpA helix in the reference frame of the other for both the wild type and all of the mutants. In each case only conformations where the helices formed a dimer were combined from all seven simulations. The Cα atoms of the reference helix from each frame were fitted onto a unique reference structure to maintain the frame of reference. Blue and red indicate low and high probabilities of finding the second monomer at that position.

distribution of the two helices (Figure 5). We shall compare the mean values of the RMSD of the WT and mutant simulations later.

The GxxxG motif has been shown to be responsible for the right-hand packing conformation of the dimer (*27, 49*). The helix−helix crossing angle for the WT simulations adopts a skewed bimodal distribution (Figure 6). The values obtained from the solution/micelle NMR structure ($\Omega = -43°$) and the solid state/bilayer structure ($\Omega = \sim -35°$) lie within this distribution; however, the modal simulation crossing angle of $\Omega = -25°$ (Table 2) is smaller than the experimental values. In order to validate the crossing angle distributions seen in the CG simulations, the crossing-angle distribution was also calculated for the ensemble of NMR GpA structures in a DPC micelle (PDB: 1AFO) as well as for the previously published AT simulations of GpA in a DPC micelle and a DMPC bilayer (*22*) (Figure S1). In all cases the helix packing is clearly right-handed, although the average values are different. This could be due to a number of reasons, e.g., differences between the micellar and lipid bilayer environments, leading to the dimer adopting a different equilibrium conformation. Although the crossing angle distributions of WT GpA overlap and therefore can be considered to be consistent, the range of values predicted by the CG simulations is larger than seen in NMR experiments. This reflects the soft nature of the coarse-grained free energy landscape but may also reflect the nature of the refinement of the ensemble of NMR structures for such a dynamic system.

Table 2: Analysis of Dimer Structure and Stability

simulation	Cα RMSD[a] (Å)	modal crossing angle Ω (deg)	$\Delta\Delta G^b$ (kJ/mol)
GpA-WT	3.6 ± 1.3	−25	
GpA-G83L	5.0 ± 1.1	15	10.9
GpA-T87F	5.1 ± 1.0	15	9.1
GpA-G79LG83L	4.3 ± 1.2	bimodal: −25 and 15	9.0
GpA-A82W	3.8 ± 1.3	bimodal: −25 and 15	3.6
GpA-I85F	3.5 ± 1.3	−25	4.4

[a] For the residues of the interaction motif (LI...T) relative to the starting (NMR) structure as the reference structure. These Cα RMSDs were calculated by deriving a single trajectory from each ensemble of simulations by concatenating the dimeric segments of the constituent trajectories of the ensemble. The overall average RMSD for an ensemble was then derived by comparing the concatenated trajectory vs the coarse-grained solution/micelle NMR structure (*10*). Similar RMSD values (not shown) were obtained by comparison with the solid state/bilayer NMR structure (*14*). [b] For details of the calculation, see Materials and Methods and the Supporting Information.

GpA Mutants. The same analysis of d_{HH} vs time was used to monitor formation of dimers in the simulations of the mutant TM helices. As with the WT simulations, the helices generally formed a dimer in the first 500 ns. The mutants, however, differed from the WT simulations and from one another in the extent to which subsequent dissociation of the dimer occurred in each simulation. In particular, the helices dissociated once or twice in four out of seven simulations for the mutants known to form unstable dimers

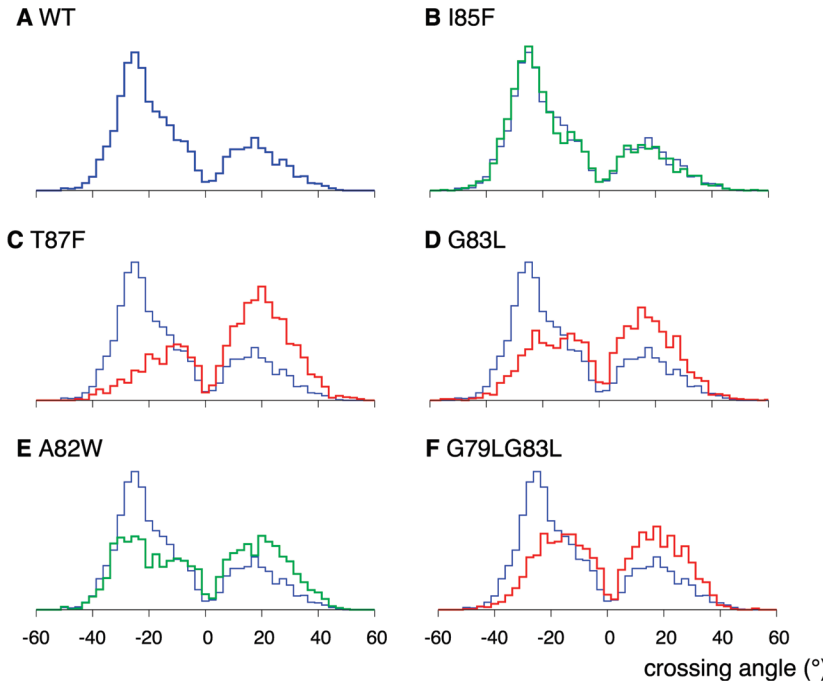

FIGURE 6: Helix crossing angle histograms. For each set of simulations only those conformations where the helices formed a dimer were extracted and merged. Helix crossing angles (Ω) were then evaluated from these merged dimer trajectories. Note that a positive crossing angle corresponds to left-handed helix packing and a negative crossing angle to right-handed packing. Since these are histograms, the area under each curve sums to unity. The wild type is drawn in blue, and the nondisruptive and disruptive mutants are drawn in green and red, respectively.

(G83L, T87F, and G79LG83L). This can also be seen in the motion of the helices in the reference frame of the lipid bilayer (Figure 4B). Again, the mobile helix appears to diffuse (i.e., move randomly) when not bound to the fixed helix either at the beginning of the simulation or when dissociated. The dimers in the simulations of the nondisruptive mutants (A82W and I85F) dissociated in fewer simulations. This suggests that comparing the behavior of the dimers and monomers might prove insightful.

The spatial distribution of the one of the helices around the other is shown in Figure 5. For the nondisruptive mutants (A82W and I85F) the spatial distribution is similar to the wild type: they all favor the same side of the fixed helix. However, for the T87F and G83L mutants, the spatial distribution is bimodal with the mobile helix preferentially found on the two opposite sides of the fixed helix although the spatial distribution of the G83L mutant is more uniform. Finally, the spatial distribution of the mobile helix of the G79LG83L mutant favors one side of the fixed helix which differs from the WT distribution. The T87F mutant is also interesting as the mobile helix does not adopt the orientation displayed by the wild-type dimer.

We can directly calculate the association equilibrium constant (and therefore the free energy of association ΔG) for the wild-type and mutant sequences from these simulations (Figure 3; see Materials and Methods and the Supporting Information for details). These values of ΔG are likely to be inaccurate because, first, it is difficult to define a standard state and, second, the experimental values were measured using detergent micelles rather than lipid bilayers, so a direct comparison is not possible. Finally, it is likely that the CG model will introduce systematic errors; for example, the interaction between two particle types not directly involved in the mutation may be over- or underestimated. This will bias the individual calculated values. Instead, we shall calculate how the free energy changes when a mutation is made ($\Delta\Delta G$). Of course, we are assuming that the magnitudes of the systematic errors are approximately constant and will therefore cancel when the values of $\Delta\Delta G$ are calculated.

The three disruptive mutants (G83L, T87F, and G79LG83L) have $\Delta\Delta G$ values of 9−11 kJ/mol (Table 2). This corresponds to an ~40× decrease in the equilibrium constant for dimerization compared to the wild-type sequence. In contrast, the two nondisruptive mutants (A82W and I85F) have $\Delta\Delta G$ values of ~4 kJ/mol, corresponding to an ~4× decrease in the equilibrium constant for dimerization. Examining the variations between simulations suggests that a $\Delta\Delta G$ of ~4 kJ/mol may not be significant; i.e., the statistical error is of the order of 4 kJ/mol. We therefore predict that $\Delta\Delta G_{T87F} \approx \Delta\Delta G_{G83L} \approx \Delta\Delta G_{G79LG83L} \gg \Delta\Delta G_{A82W} \approx \Delta\Delta G_{I85F}$. This order is consistent with the patterns of dimer destabilization seen in mutational experimental studies. We describe this analysis as semiquantitative since not only does it yield a predicted order for the values of $\Delta\Delta G$ but it is also able to give approximate magnitudes.

This semiquantitative correlation between our simulations and experiment is encouraging. Using simulation we may investigate the microscopic causes of the observed differences in the association free energy. We first analyzed the behavior of GpA in the bilayer environment. It was observed that the positions along the bilayer normal for both helices were almost identical for either the WT or the mutant GpA simulations in both the monomeric and dimeric states. The mean tilt angle of the helices with respect to the bilayer normal was also calculated for these states. Again, the behavior was similar for the WT and each of the mutant

simulations in both the monomeric and dimeric states. In all cases the mean tilt angle was in the range 16−17°.

We shall now compare the RMSDs of the dimer interaction motif formed by the various mutants (Table 2) relative to the NMR structures. We note that whereas the nondisruptive mutants (A82W and I85F) have similar RMSDs (ca. 3.6 Å) to the WT simulation, two of the disruptive mutant simulations (G83L and T87F) yield much higher RMSDs (ca. 5 Å). The RMSD (4.3 Å) of the remaining disruptive mutant (G79LG83L) was slightly less than the other two, but still significantly higher than the nondisruptive mutants and the wild type. For reference, the RMSD values for the key motif residues of each individual helix monomer for both the WT and mutant simulations were all between 1.3 and 1.4 Å. Thus, the elevated RMSDs reflect changes in interhelix, not intrahelix, interactions as indicated by Figure 5. Since these RMSDs correspond only to those segments of each simulation where a dimer (as judged by d_{HH}) is present, this indicates that not only do the disruptive mutants lead to a less stable (i.e., high $\Delta\Delta G$) dimer but also the structure of the dimer differs significantly from that of the wild type.

We may also compare the distribution of crossing angles (Ω) for the various mutants to explore the degree of disruption of the helix−helix interface observed in the simulations (Figure 6 and Table 2). All three disruptive mutants result in a significant shift, relative to the WT, from a right-handed (Ω negative) to a left-handed (Ω positive) distribution. Interestingly, for both the G83L and G79LG83L mutants the distribution is more bimodal than the WT distribution, suggesting that these disruptive mutants "soften" the interhelix interface. The crossing angle distribution of the nondisruptive mutant I85F is almost identical to that of the WT simulations, indicating that this mutation does not significantly perturb the dimer. For the A82W mutant the situation is a little more complex; this is discussed in more detail below.

The structural consequence of these changes may be explored in more detail by analyzing the residues that form the contacts between the helices (as for the WT in Figure 2B; data not shown for mutant simulations) and by visual inspection of individual structures (Figure 7) selected to correspond to the modal crossing angles in Figure 6. For the nondisruptive mutants (A82W and I85F) the pattern formed by the residues closer than 8 Å to one another is similar to the WT simulations (see above); this corresponds closely with the pattern of contacts observed in the NMR structure. For the A82W mutant, however, structures are also seen with a left-handed packing of helices. This correlates with the formation of a contact that is not seen in the WT simulations between the mutated residue (i.e., W82) and T87. T87 is the only polar side chain within the dimerization motif and has been shown to be important for dimer stability (*30*). Our simulations suggest that the side chain of W82 is able to interact with T87 residues on both the opposing helix and on the same helix. This partially "unlocks" the critical T87−T87 interaction, as confirmed by the observation that the propensity for the crossing of the helices to be right-handed is to some extent lost, resulting in an approximately symmetrical bimodal distribution (Figure 6), with crossing angle modes of ∼−25° (left-handed) and ∼+15° (right-handed).

For both the G83L and T87F mutants the helix packing is perturbed relative to the WT simulations such that the preferred crossing angle becomes ∼+15°, i.e., a left-handed dimer (see above). The loss of the key Thr−Thr polar interaction in T87F, but the preservation of a bulky side chain in this position, results in the loss of bias toward right-handedness, and all of the important contacts around the dimerization motif are also lost. For the T87F mutant contact analysis revealed that no specific, long-lived interactions are observed along the helix−helix interface, consistent with the relative instability of this dimer relative to the wild type. This confirms the importance of T87 in maintaining a strong helix−helix interface.

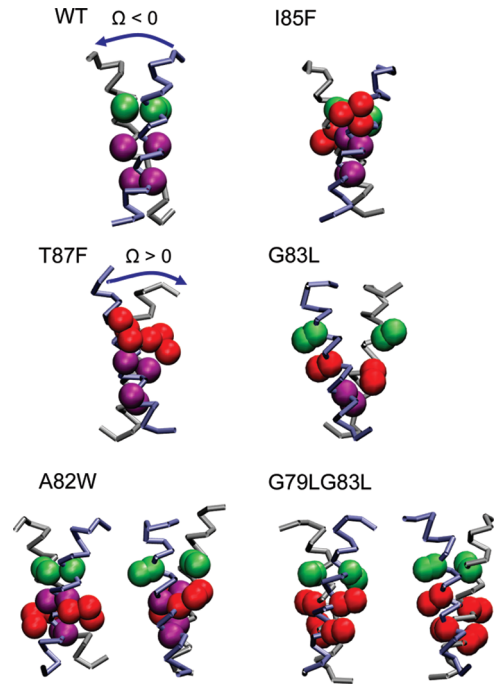

FIGURE 7: Structures of WT and mutant helix dimers. Structures were selected to be representative of the modes in the crossing angle distributions. The backbones of the two helices are in silver and blue. The G79 and G83 backbone particles are shown in purple, the backbone and side chain particles of the T87 particles in green, and the mutated residues in red.

The tight dimerization interface observed in the GpA-WT is lost upon mutation of one or two of the key Gly residues. For example, when two key Gly residues in the dimerization motif are removed (G79LG83L), a symmetrical crossing angle distribution is observed (above). Thus, the helices do not have a preferred packing handedness and fluctuate between two values. The G79 and G83 residues in the WT structure provide stabilizing Gly−Gly interactions as well as allowing the close approach of other nearby residue side chains within the motif. Thus, in the double mutant there are relatively few contacts between the helices within 8 Å. Extending the cutoff to 10 Å increases the number of interactions observed, some of which are shifted approximately one residue along from the usual pattern of interactions observed for the WT simulations; these include I76, V80, and V84. The weakness of these interactions evidently reduces the strength of the dimerization interface and removes the crossing angle bias.

DISCUSSION

Our key finding is that one can use CG-MD to characterize the effect of mutations on the stability and structure of TM

helix dimers, thus providing a possible approach to modeling the packing of TM helices. This is of relevance both to ongoing efforts to understand the relationship between membrane protein structure and stability (reviewed in ref *4*) and to use computational methods to aid the interpretation and modeling of low-resolution membrane protein structural data. Examination of the structures generated by the CG-MD method for the WT and nondisruptive mutants suggests that, on average, the NMR structure is preserved. This is consistent with our earlier studies in which a lipid bilayer was self-assembled in the presence of two TM helices.

When CG-MD is used to explore dimerization of disruptive mutants, two key effects are seen. First, the mutant dimer is destabilized relative to the WT dimer, although even in the most disruptive mutant (G83L) the dimer still forms (see below). Second, if one examines the structures (e.g., the helix−helix contacts and crossing angles) of the dimers for the disruptive mutants, the structure is perturbed relative to that of the wild type.

It is useful to compare these results with previous experimental and computational studies of glycophorin dimerization. The mutants that were simulated in this study were selected on the basis of earlier studies of the glycophorin dimerization interface (*8, 28*). Our results are in agreement with these essentially qualitative data. There is also a wealth of more quantitative data available for the free energies of GpA TM helix dimerization in detergent micelles and the effects of mutation on the dimerization free energy (*50*−*53*). Initial analytical ultracentrifugation studies of the monomer−dimer equilibrium for GpA TM helices in detergent (pentaoxyethylene octyl ether, C_8E_5) micelles revealed that even for disruptive mutants significant amounts of dimer were present (*50*), in contrast with the situation in sodium dodecylsulfate (SDS) (*28*). This is of interest, as in the current study we also observed significant dimer formation even for the disruptive mutants. It is also possible to compare the $\Delta\Delta G$ values from the current simulations with those from the ultracentrifugation studies (*51*−*53*). Thus, for the G83L mutant the simulation value of $\Delta\Delta G$ of +11 kJ/mol is comparable to the experimental value of +14 kJ/mol. Given the semiquantitative nature of the simulation, and the observed dependence of the ΔG of dimerization on the experimental environment (*54*), such agreement is most encouraging. Looking at the other disruptive mutants, we estimate a $\Delta\Delta G$ of +9 kJ/mol for T87F compared to an experimental value of +13 kJ/mol for T87L, and for G79LG83L we estimate +9 kJ/mol compared to +15 kJ/mol for G79AG83A.

There is also a considerable computational literature on GpA modeling and simulations, e.g., refs *16*−*18*, *21*, *23*, and *55*−*59*. A number of relatively simple computational models have been able to predict/reproduce the overall structure of the GpA helix dimer, e.g., refs *23* and *55*. This suggests that this structure is dominated by van der Waals/packing interactions, which are captured in many such models. It is encouraging that a number of different models can also yield information on the effects of mutants, e.g., refs *21*, *58* and *60*. It is of interest that these include a highly coarse-grained approach which treats each amino acid as a single particle (*60*), suggesting that atomistic detail may not be necessary for an accurate predictive model. All atom MD simulations, albeit in a membrane mimetic dodecane slab, have been used to compute dimerization $\Delta\Delta G$ values for mutants: these estimated values of $\Delta\Delta G$ for the I76A mutant of +6 kJ/mol (*21*) compare well with the experimental value of +8 kJ/mol (*53*). Atomistic MD, CG-MD, and experimental approaches therefore yield comparable estimates of the $\Delta\Delta G$ of dimerization for disruptive mutants.

It is important to explore the possible advantages of this approach, which seems to work well at a semiquantitative level. The main difference from AT-MD simulations is that it is computationally cheaper (by ∼100×), thus allowing either larger systems to be studied or a large number of mutants of a single protein to be screened in a high throughput manner. At the same time, compared to approaches which treat the bilayer as a low dielectric continuum (e.g., ref *17*) the CG-MD method retains some details of the lipid bilayer headgroups. Given the observed influence of, e.g., detergent species (*12, 15, 54*) on GpA dimerization, we suggest that this degree of realism may be an important feature in future studies of membrane protein stability, self-assembly, and folding.

In addition to being of relevance to α-helix association as a component of membrane protein folding, this simulation approach may be of broader biochemical significance. Thus, GxxxG motifs have been implicated in transmembrane helix dimerization of a number of signaling proteins, including integrins (*61*), syndecans (*62*), and the ErbB family of receptors (*63*). It will therefore be of interest to explore helix dimerization in wild types vs mutants for these systems.

Of course, there are number of limitations to the CG approach. In particular in the context of GpA dimerization, it does not contain atomistic detail and so cannot, for example, capture the possible role of Cα−H···O H-bonds (*64*). This, along with the discrete nature of other interactions, leads to the free energy interaction landscape being smoother than the atomistic equivalent. We purposefully chose mutants which had either a significant effect or, in the case of the controls, no effect on dimerization so as to maximize the probability that the CG model could discriminate between them. Conversely, we do not expect the CG approach to work when the mutation does not significantly alter the chemistry or size of the amino acid, for example, valine to isoleucine, since the difference in CG parameters is small. The broad range of crossing angles observed from the CG simulations may also be due to this effect. However, we cannot rule out other factors, such as the difficulty in determining NMR structures of α-helical membrane proteins or inaccuracies in the CG force field itself. Despite this we obtained a good semiquantitative agreement between our calculated $\Delta\Delta G$ values and published experimental data. We emphasize that the value in this approach is in the comparison between the behavior of different GpA sequences; for example, we predict that the T87F mutant forms left-handed dimers.

At present we would therefore describe the CG approach as semiquantitative although the agreement with experiment is good. It will be of interest to see how improved CG force fields (*41*) may alter this. However, in the longer term the solution to the limitations of CG methods may be to combine CG and all-atom (AT) models together in a multiscale approach (*65*). This would combine the predictive potential of CG approaches with the ability of extended AT-MD simulations to refine initial structural models of TM helix packing (*22*). Moreover, future work will include CG

simulations where more than two GpA helices will be present in the starting structure in order to investigate if the dimers will dominate.

Overall, these studies demonstrate that CG-MD can be used to explore the interactions of TM helices, an important stage in the folding of membrane proteins. In particular, CG-MD has been shown to be sensitive enough to detect disruptions introduced by mutation, suggesting that CG-MD may be used as a key component within a multiscale approach that uses simulation to predict the folding of membrane proteins.

SUPPORTING INFORMATION AVAILABLE

A derivation of the relationship between macroscopic thermodynamics and single molecular observations from simulations of TM helix dimerization and helix crossing angle distributions comparing the WT GpA dimer in CG simulations in a DPPC lipid bilayer, in the NMR structure ensemble (PDB: 1AFO), in a DPC detergent micelle, and in AT simulations in both a DMPC lipid bilayer and a DPC detergent micelle. This material is available free of charge via the Internet at http://pubs.acs.org.

REFERENCES

1. Hurwitz, N., Pellegrini-Calace, M., and Jones, D. T. (2006) Towards genome-scale structure prediction for transmembrane proteins. *Philos. Trans. R. Soc. B 361*, 465–475.
2. Engelman, D. M., Chen, Y., Chin, C., Curran, R., Dixon, A. M., Dupuy, A., Lee, A., Lehnert, U., Mathews, E., Reshetnyak, Y., Senes, A., and Popot, J. L. (2003) Membrane protein folding: beyond the two stage model. *FEBS Lett. 555*, 122–125.
3. Fleishman, S. J., Unger, V. M., and Ben-Tal, N. (2006) Transmembrane protein structures without X-rays. *Trends Biochem. Sci. 31*, 106–113.
4. Senes, A., Engel, D. E., and DeGrado, W. F. (2004) Folding of helical membrane proteins: the role of polar, GxxxG-like and proline motifs. *Curr. Opin. Struct. Biol. 14*, 465–479.
5. Deber, C. M., and Therien, A. G. (2002) Putting the b-breaks on membrane protein misfolding. *Nat. Struct. Biol. 9*, 318–319.
6. van den Berg, B., Clemons, W. M., Collinson, I., Modis, Y., Hartmann, E., Harrison, S. C., and Rapoport, T. A. (2004) X-ray structure of a protein-conducting channel. *Nature 427*, 36–44.
7. Bowie, J. U. (2005) Solving the membrane protein folding problem. *Nature 438*, 581–589.
8. Treutlein, H. R., Lemmon, M. A., Engelman, D. M., and Brunger, A. T. (1992) The glycophorin A transmembrane domain dimer: Sequence specific propensity for a right handed supercoil of helices. *Biochemistry 31*, 12726–12733.
9. Langosch, D., Brosig, B., Kolmar, H., and Fritz, H. J. (1996) Dimerisation of the glycophorin A transmembrane segment in membranes probed with the ToxR transcription activator. *J. Mol. Biol. 263*, 525–530.
10. MacKenzie, K. R., Prestegard, J. H., and Engelman, D. M. (1997) A transmembrane helix dimer: structure and implications. *Science 276*, 131–133.
11. Brosig, B., and Langosch, D. (1998) The dimerization motif of the glycophorin A transmembrane segment in membranes: importance of glycine residues. *Protein Sci. 7*, 1052–1056.
12. Fisher, L. E., Engelman, D. M., and Sturgis, J. N. (1999) Detergents modulate dimerization, but not helicity, of the glycophorin A transmembrane domain. *J. Mol. Biol. 293*, 639–651.
13. Popot, J. L., and Engelman, D. M. (2000) Helical membrane protein folding, stability, and evolution. *Annu. Rev. Biochem. 69*, 881–922.
14. Smith, S. O., Song, D., Shekar, S., Groesbeek, M., Ziliox, M., and Aimoto, S. (2001) Structure of the transmembrane dimer interface of glycophorin A in membrane bilayers. *Biochemistry 40*, 6553–6558.
15. Fisher, L. E., Engelman, D. M., and Sturgis, J. N. (2003) Effect of detergents on the association of the glycophorin a transmembrane helix. *Biophys. J. 85*, 3097–3105.
16. Petrache, H. I., Grossfield, A., MacKenzie, K. R., Engelman, D. M., and Woolf, T. B. (2000) Modulation of glycophorin A transmembrane helix interactions by lipid bilayers: Molecular dynamics calculations. *J. Mol. Biol. 302*, 727–746.
17. Im, W., Feig, M., and Brooks, C. L. (2003) An implicit membrane generalized Born theory for the study of structure, stability, and interactions of membrane proteins. *Biophys. J. 85*, 2900–2918.
18. Kim, S., Chamberlain, A. K., and Bowie, J. U. (2003) A simple method for modeling transmembrane helix oligomers. *J. Mol. Biol. 329*, 831–840.
19. Braun, R., Engelman, D. M., and Schulten, K. (2004) Molecular dynamics simulations of micelle formation around dimeric Glycophorin A transmembrane helices. *Biophys. J. 87*, 754–763.
20. Kokubo, H., and Okamoto, Y. (2004) Prediction of membrane protein structures by replica-exchange Monte Carlo simulations: Case of two helices. *J. Chem. Phys. 120*, 10837–10847.
21. Hénin, J., Pohorille, A., and Chipot, C. (2005) Insights into the recognition and association of transmembrane a-helices. The free energy of α-helix dimerization in glycophorin A. *J. Am. Chem. Soc. 127*, 8478–8484.
22. Cuthbertson, J. M., Bond, P. J., and Sansom, M. S. P. (2006) Transmembrane helix-helix interactions: comparative simulations of the glycophorin A dimer. *Biochemistry 45*, 14298–14310.
23. Efremov, R. G., Vereshaga, Y. A., Volynsky, P. E., Nolde, D. E., and Arseniev, A. S. (2006) Association of transmembrane helices: what determines assembling of a dimer? *J. Comput.-Aided Mol. Des. 20*, 27–45.
24. Beevers, A. J., and Kukol, A. (2006) Systematic molecular dynamics searching in a lipid bilayer: application to the glycophorin A and oncogenic ErbB-2 transmembrane domains. *J. Mol. Graphics Modelling 25*, (in press).
25. Bond, P. J., and Sansom, M. S. P. (2006) Insertion and assembly of membrane proteins via simulation. *J. Am. Chem. Soc. 128*, 2697–2704.
26. Smith, S. O., Eilers, M., Song, D., Crocker, E., Ying, W., Groesbeek, M., Metz, G., Ziliox, M., and Aimoto, S. (2002) Implications of threonine hydrogen bonding in the glycophorin A transmembrane helix dimer. *Biophys. J. 82*, 2476–2486.
27. Russ, W. P., and Engelman, D. M. (2000) The GxxxG motif: a framework for transmembrane helix-helix association. *J. Mol. Biol. 296*, 911–919.
28. Lemmon, M. A., Flanagan, J. M., Treutlein, H. R., Zhang, J., and Engelman, D. M. (1992) Sequence specificity in the dimerisation of transmembrane α-helices. *Biochemistry 31*, 12719–12725.
29. Lemmon, M. A., Treutlein, H. R., Adams, P. D., Brunger, A. T., and Engelman, D. M. (1994) A dimerisation motif for transmembrane a helices. *Nat. Struct. Biol. 1*, 157–163.
30. MacKenzie, K. R., and Engelman, D. M. (1998) Structure-based prediction of the stability of transmembrane helix-helix interactions: the sequence dependence of glycophorin A dimerization. *Proc. Natl. Acad. Sci. U.S.A. 95*, 3583–3590.
31. Bond, P. J., and Sansom, M. S. P. (2003) Membrane protein dynamics vs. environment: simulations of OmpA in a micelle and in a bilayer. *J. Mol. Biol. 329*, 1035–1053.
32. Gumbart, J., Wang, Y., Aksimentiev, A., Tajkhorshid, E., and Schulten, K. (2005) Molecular dynamics simulations of proteins in lipid bilayers. *Curr. Opin. Struct. Biol. 15*, 423–431.
33. Bond, P. J., Cuthbertson, J. M., Deol, S. D., and Sansom, M. S. P. (2004) MD simulations of spontaneous membrane protein/detergent micelle formation. *J. Am. Chem. Soc. 126*, 15948–15949.
34. Dell'Orco, D., De Benedetti, P. G., and Fanelli, F. (2007) In silico screening of mutational effects on transmembrane helix dimerization: insights from rigid body docking and molecular dynamics simulations. *J. Phys. Chem. B 111*, 9114–9124.
35. Stockner, T., Ash, W. L., MacCallum, J. L., and Tieleman, D. P. (2004) Direct simulation of transmembrane helix association: role of asparagines. *Biophys. J. 87*, 1650–1656.
36. Shelley, J. C., Shelley, M. Y., Reeder, R. C., Bandyopadhyay, S., and Klein, M. L. (2001) A coarse grain model for phospholipid simulations. *J. Phys. Chem. B 105*, 4464–4470.
37. Marrink, S. J., de Vries, A. H., and Mark, A. E. (2004) Coarse grained model for semiquantitative lipid simulations. *J. Phys. Chem. B 108*, 750–760.
38. Nielsen, S. O., Lopez, C. F., Srinivas, G., and Klein, M. L. (2004) Coarse grain models and the computer simulation of soft materials. *J. Phys.: Condens. Matt. 16*, R481−R512.
39. Shih, A. Y., Arkhipov, A., Freddolino, P. L., and Schulten, K. (2006) Coarse grained protein-lipid model with application to lipoprotein particles. *J. Phys. Chem. B 110*, 3674–3684.

40. Bond, P. J., Holyoake, J., Ivetac, A., Khalid, S., and Sansom, M. S. P. (2007) Coarse-grained molecular dynamics simulations of membrane proteins and peptides. *J. Struct. Biol. 157*, 593–605.
41. Marrink, S. J., Risselada, J., Yefimov, S., Tieleman, D. P., and de Vries, A. H. (2007) The MARTINI forcefield: coarse grained model for biomolecular simulations. *J. Phys. Chem. B 111*, 7812–7824.
42. Sansom, M. S. P., Scott, K. A., and Bond, P. J. (2008) Coarse grained simulation: a high throughput computational approach to membrane proteins. *Biochem. Soc. Trans. 36*, 27–32.
43. Sanchez, R., and Sali, A. (2000) Comparative protein structure modeling. Introduction and practical examples with modeller. *Methods Mol. Biol. 143*, 97–129.
44. Lindahl, E., Hess, B., and van der Spoel, D. (2001) GROMACS 3.0: a package for molecular simulation and trajectory analysis. *J. Mol. Modelling 7*, 306–317.
45. Bond, P. J., Wee, C. L., and Sansom, M. S. P. (2008) Coarse-grained molecular dynamics simulations of the energetics of helix insertion into a lipid bilayer. *Biochemistry* (in press).
46. Bond, P. J., and Sansom, M. S. P. (2007) Bilayer deformation by the Kv channel voltage sensor domain revealed by self-assembly simulations. *Proc. Natl. Acad. Sci. U.S.A. 104*, 2631–2636.
47. Berendsen, H. J. C., Postma, J. P. M., van Gunsteren, W. F., DiNola, A., and Haak, J. R. (1984) Molecular dynamics with coupling to an external bath. *J. Chem. Phys. 81*, 3684–3690.
48. Humphrey, W., Dalke, A., and Schulten, K. (1996) VMD—Visual Molecular Dynamics. *J. Mol. Graphics 14*, 33–38.
49. Senes, A., Gerstein, M., and Engelman, D. M. (2000) Statistical analysis of amino acid patterns in transmembrane helices: The GxxxG motif occurs frequently and in association with beta-branched residues at neighboring positions. *J. Mol. Biol. 296*, 921–936.
50. Fleming, K. G., Ackerman, A. L., and Engelman, D. M. (1997) The effect of point mutations on the free energy of transmembrane α helix dimerization. *J. Mol. Biol. 272*, 266–275.
51. Fleming, K. G., and Engelman, D. M. (2001) Specificity in transmembrane helix-helix interactions can define a hierarchy of stability for sequence variants. *Proc. Natl. Acad. Sci. U.S.A. 98*, 14340–14344.
52. Doura, A. K., and Fleming, K. G. (2004) Complex interactions at the helix-helix interface stabilize the glycophorin A transmembrane dimer. *J. Mol. Biol. 343*, 1487–1497.
53. Doura, A. K., Kobus, F. J., Dubrovsky, L., Hibbard, E., and Fleming, K. G. (2004) Sequence context modulates the stability of a GxxxG-mediated transmembrane helix-helix dimer. *J. Mol. Biol. 341*, 991–998.
54. Fleming, K. G., Ren, C. C., Doura, A. K., Eisley, M. E., Kobus, F. J., and Stanley, A. M. (2004) Thermodynamics of glycophorin A transmembrane helix dimerization in C14 betaine micelles. *Biophys. Chem. 108*, 43–49.
55. Fleishman, S. J., and Ben-Tal, N. (2002) A novel scoring function for predicting the conformations of tightly packed pairs of transmembrane alpha-helices. *J. Mol. Biol. 321*, 363–378.
56. Pohorille, A., Wilson, M. A., and Chipot, C. (2003) Membrane peptides and their role in protobiological evolution. *Origins Life Evol. Biosphere 33*, 173–197.
57. Mottamal, M., Zhang, J., and Lazaridis, T. (2006) Energetics of native and non-native states of the glycophorin transmembrane helix dimer. *Proteins: Struct., Funct., Bioinf. 62*, 996–1009.
58. Metcalf, D. G., Law, P. B., and DeGrado, W. F. (2007) Mutagenesis data in the automated prediction of transmembrane helix dimers. *Proteins: Struct., Funct., Bioinf. 67*, 375–384.
59. Enosh, A., Fleishman, S. J., Ben-Tal, N., and Halperin, D. (2007) Prediction and simulation of motion in pairs of transmembrane alpha-helices. *Bioinformatics 23*, E212−E218.
60. Park, Y., Elsner, M., Staritzbichler, R., and Helms, V. (2004) Novel scoring function for modeling structures of oligomers of transmembrane alpha-helices. *Proteins: Struct., Funct., Bioinf. 57*, 577–585.
61. Li, R., Mitra, N., Gratkowski, H., Vilaire, G., Litvinov, R., Nagasami, C., Weisel, J. W., Lear, J. D., DeGrado, W. F., and Bennett, J. S. (2003) Activation of integrin alphaIIbbeta3 by modulation of transmembrane helix associations. *Science 300*, 795–798.
62. Dews, I. C., and MacKenzie, K. R. (2007) Transmembrane domains of the syndecan family of growth factor coreceptors display a hierarchy of homotypic and heterotypic interactions. *Proc. Natl. Acad. Sci. U.S.A. 104*, 20782–20787.
63. Landau, M., and Ben-Tal, N. (2008) Dynamic equilibrium between multiple active and inactive conformations explains regulation and oncogenic mutations in ErbB receptors. *Biochim. Biophys. Acta 1785*, 12–31.
64. Senes, A., Ubarretxena-Belandia, I., and Engelman, D. M. (2001) The Cα—H···O hydrogen bond: a determinant of stability and specificity in transmembrane helix interactions. *Proc. Natl. Acad. Sci. U.S.A. 98*, 9056–9061.
65. Shi, Q., Izvekov, S., and Voth, G. A. (2006) Mixed atomistic and coarse-grained molecular dynamics: simulation of a membrane bound ion channel. *J. Phys. Chem. B 110*, 15045–15048.

BI800678T